REGULAR ARTICLE

blood advances

Nilotinib attenuates vascular pathology in experimental cerebral malaria

Luana S. Ortolan,[1,*] Priyanka Bansal,[1,*] Veronica I. Primavera,[1] Rodrigo J. R. X. Freitas,[2] Ling Wei,[1] Sabrina Epiphanio,[3] Alexis Kaushansky,[1,4] and Joseph D. Smith[1,4]

[1]Center for Global Infectious Disease Research, Seattle Children's Research Institute, Seattle, WA; [2]Department of Immunology, Institute of Biomedical Sciences, and [3]Department of Clinical and Toxicological Analyses, Faculty of Pharmaceutical Sciences, University of Sao Paulo, Sao Paulo, Brazil; and [4]Department of Pediatrics, University of Washington, Seattle, WA

Key Points

- BCR-ABL drugs differentially modulate parasite and thrombin-induced activation of human brain endothelial cells.
- Nilotinib reduces vascular pathology in mice with experimental CM.

Cerebral malaria (CM), a life-threatening complication of *Plasmodium falciparum* infection, is characterized by the sequestration of infected erythrocytes in the brain microvasculature. Our study investigated the potential of repurposing tyrosine kinase inhibitors targeting BCR-ABL1 (BCR-ABL drugs), which are also known to be effective against *P falciparum* blood-stage parasites, for mitigating inflammation and blood-brain barrier breakdown in CM. Our analysis demonstrated differential protective effects of BCR-ABL drugs on primary human brain microvascular endothelial cells exposed to thrombin or a *P falciparum*-infected erythrocyte challenge. Bosutinib attenuated both thrombin- and parasite-induced barrier alterations, whereas nilotinib was only effective against thrombin, and imatinib protected against neither. Bosutinib's barrier protective effect was associated with reduced interendothelial gap formation and decreased phosphorylation of the adherens junction protein VE-cadherin and the focal adhesion protein paxillin. In the mouse experimental CM model, nilotinib showed superior efficacy over imatinib and bosutinib. In mice, nilotinib led to fewer brain hemorrhages and less vascular congestion than the antimalaria drug artesunate at similar levels of parasitemia control. Our findings provide important mechanistic insight into the activities of BCR-ABL drugs to suppress endothelial barrier disruptive signaling in vitro and to protect in a mouse model of CM. These findings can inform the repurposing of these drugs in malaria treatment, particularly for managing cerebral complications.

Introduction

Vascular dysfunction, characterized by endothelial activation and vascular leak, is observed with hyperinflammatory infectious diseases.[1-3] However, there are limited therapeutic approaches for repairing and stabilizing the endothelial barrier following inflammatory damage. Cerebral malaria (CM) is a severe complication of *Plasmodium falciparum* infection that kills hundreds of thousands of African children each year[4] and can lead to long-term neurologic and cognitive impairments in survivors.[5,6] Despite the success of the fast-acting antimalaria drug artesunate in improving patient survival,[7]

Submitted 14 November 2024; accepted 16 February 2025; prepublished online on *Blood Advances* First Edition 24 February 2025. https://doi.org/10.1182/bloodadvances.2024015364.

*L.d.S.O. and P.B. contributed equally to this work.

Original data are available on request from the corresponding author, Joseph D. Smith (joe.smith@seattlechildrens.org).

The full-text version of this article contains a data supplement.

there remains a substantial need to identify adjunctive drug therapies to attenuate hyperinflammatory injury present in severe malaria.

The pathology of CM is characterized by the sequestration of *P falciparum*–infected erythrocytes (Pf-IEs) in the brain microvasculature,[8,9] which leads to blood flow obstruction, ischemia, and brain swelling.[10] This sequestration promotes endothelial dysfunction and blood-brain barrier disruption through a combination of parasite factors,[11-15] dysregulation of coagulation,[16] and cytokine storm.[2,17,18] Moreover, CM isolates adhere to endothelial protein C receptor (EPCR),[19-24] a crucial anti-inflammatory receptor on blood vessels. Parasite binding disrupts its interaction with protein C and impairs the regulation of thrombin-induced signaling in endothelial cells.[25-27] Postmortem brain histology revealed co-localization of thrombin, fibrin deposits, and Pf-IEs in cerebral microvessels,[28,29] accompanied by EPCR loss,[16] which point to complex interactions between thrombin and secreted parasite inflammatory stimuli that drive endothelial dysfunction in CM.

Host-directed therapies for malaria represent a promising strategy to overcome parasite drug resistance and counteract inflammation in severe malaria.[2,30-32] Recent studies have demonstrated that BCR-ABL1 tyrosine kinase inhibitors (hereafter referred to as BCR-ABL drugs), originally developed for chronic myelogenous leukemia treatment,[33] effectively inhibit *P falciparum* growth in erythrocytes.[34-36] Moreover, imatinib has shown safety and efficacy in accelerating *P falciparum* clearance in human adults with uncomplicated malaria.[37] Beyond antiparasitic effects, BCR-ABL drugs are being investigated for their potential to address endothelial dysfunction and vascular leak in murine models of sepsis.[38-40] Some BCR-ABL drugs have demonstrated the ability to attenuate thrombin-induced permeability in primary human brain microvascular endothelial cells (HBMECs)[41] and to exhibit anti-inflammatory activity in the mouse experimental CM (ECM) model.[42,43] Taken together, these findings suggest that modulating kinase signaling pathways may offer a dual benefit by enhancing parasitemia control while simultaneously reducing inflammatory damage to blood vessels.

This study evaluated BCR-ABL drugs using primary HBMEC in vitro assays and a mouse ECM model.[44,45] Our analysis revealed different barrier protective activities among the BCR-ABL drug family members against thrombin and Pf-IE stimuli. Notably, nilotinib diminished brain vascular pathology in mice, both as a monotherapy and in combination with the antimalarial drug artesunate.

Methods

P falciparum culture and 2-cycle in vitro growth inhibition assay

P falciparum 3D7 and IT4var19 (DC8-EPCR) parasites were cultured and synchronized according to standard procedures.[19] Lysates of uninfected red blood cells or purified mature stage *P falciparum* parasite IEs were prepared by 5 freeze-thaw cycles using dry ice and a 37°C water bath. Lysates from 2 × 10^6 IEs per cm^2 were used for HBMECs monolayer for xCELLigence and western blot assays. Enrichment of mature schizont-IEs was achieved using Low-Density and Magnetic Activated Cell Sorting (LD-MACS) magnetic purification (25 LD columns, Miltenyi Biotec, Germany). For parasite-drug viability assays, we used a 2-cycle *P falciparum* growth inhibition assay. Ring-stage (12-hour) Pf-IEs were treated with BCR-ABL drugs at different concentrations. To measure parasite viability, parasitemia was evaluated using flow cytometry after 60 hours of drug treatment (72-hour time point) using SYBR Green I DNA stain (Invitrogen), and the data were subsequently analyzed using FlowJo software. To assess parasite morphology after the drug treatments, blood smears were fixed with methanol, stained with 5% Giemsa, and images were acquired using brightfield microscopy at magnification ×100 with a Keyence microscope (Keyence Corporation).

Human brain microvascular endothelial cell culture

Primary HBMECs (Cell Systems; catalog no. ACBRI 376) were cultured on rat tail collagen type I (5 μg/cm^2) in Endothelial Cell Growth Medium 2 (EGM-2) Basal Medium (Lonza) supplemented with Endothelial Cell Growth Medium-2MV (EGM-2MV) Microvascular Endothelial Cell Growth Medium SingleQuots (Lonza) and 5% fetal calf serum at 37°C and 5% CO_2. HBMECs were obtained at passage 3 and used until passage 9.

xCELLigence barrier assay

HBMECs at 10 000 to 12 000 cells per well were grown to confluency for 3 days in rat collagen type I precoated xCELLigence 96 PET E-plates (Agilent Technologies). For thrombin perturbation, cells were treated with 5 nM thrombin (Sigma-Aldrich) for 7 minutes, followed by the addition of 0.5 μM kinase inhibitors (KIs; Selleck Chemicals; supplemental Table 1) in triplicate wells. For parasite perturbations, KIs (0.5 μM) and lysates prepared from 2 × 10^6/cm^2 mature-stage 3D7 Pf-IEs were added together to the HBMEC monolayer. Alternatively, magnet-purified schizont stage IT4var19-IEs and KIs (0.5 μM) were added at the same time to the HBMEC monolayer. To record change in barrier properties, the cell index was measured every minute for the first 2 hours and, thereafter, every 5 minutes for 4 hours. The cell index was monitored and analyzed as detailed in the supplemental Methods.

Immunofluorescence microscopy

HBMECs were seeded at 12 000 cells per well in collagen type I–coated 8-chamber slides (Corning BioCoat). For thrombin perturbation, the cells were treated with 5 nM thrombin for 7 minutes, followed by the addition of KIs (0.5 μM). After the indicated times, HBMECs were fixed in 3.7% paraformaldehyde for 30 minutes, followed by 3 phosphate-buffered saline (PBS) washes. HBMECs were immunofluoretically stained for VE-cadherin, phalloidin, and DAPI (4′,6-diamidino-2-phenylindole) in different treatment conditions and analyzed as detailed in the supplemental Methods.

Western blot

HBMECs were seeded in 12-well plates at 24 000 cells per well and grown until confluence for 3 days. For thrombin perturbation, cells were treated with 5 nM thrombin for 7 minutes, followed by treatment with KIs (0.5 μM). For parasite perturbations, KIs (0.5 μM) and lysates prepared from 2 × 10^6/cm^2 mature-stage 3D7 Pf-IEs were added together to the HBMEC monolayer. After incubation, HBMECs were lysed, proteins were separated by electrophoresis, and transferred to polyvinylidene fluoride (PVDF) membranes for antibody staining. The blots were imaged using Bio-Rad ChemiDoc imaging system, and signals were quantified by densitometry using

ImageJ v1.53q (National Institutes of Health; https://imagej.nih.gov/ij/). Western blots were analyzed as detailed in the supplemental Methods.

Assessments of BCR-ABL drugs in the mouse ECM model

C57BL/6 female mice at 7 to 10 weeks old were purchased from the Jackson Laboratories and were acclimated for at least 3 days before experimental manipulation. The parasite strain *P berghei* ANKA (PbANKA) was supplied by Tracey J. Lamb.[42] The mice were infected intraperitoneally with 0.5×10^6 PbANKA. Body weights and blood smear parasitemia were monitored daily. Clinical scores were assessed twice a day starting on day 5 after infection using an adapted 20-point rapid murine coma and behavior scale (RMCBS).[46] As a humane end point, mice were euthanized at an RMCBS of ≤5, because they were likely to die within hours.[46] Imatinib (STI571 mesylate, Selleckchem) was diluted to a final concentration of 150 mg/kg in PBS and administered by oral gavage (OG) in a 100 μL suspension in PBS. Bosutinib (SKI-606, Selleckchem) was reconstituted in a solution buffer (2% dimethyl sulfoxide [DMSO], 30% polyethylene glycol, 5% Tween in Milli-Q water) to 50 mg/mL and administered to mice via intraperitoneal (IP) injections at a dose of 100 mg/kg per day in a 100 μL suspension of 1× PBS. Nilotinib (AMN-107, Selleckchem) was dissolved in PBS and given via OG at a dose of 100 mg/kg per day in a 100 μL suspension. Control mice received either the nilotinib vehicle (PBS) through OG or the bosutinib vehicle (2% DMSO, 30% polyethylene glycol, 5% Tween in Milli-Q water) through IP injection. Artesunate (A3731, Sigma) was resuspended in PBS and provided to infected mice from day 6 to 10 after infection in the late-stage treatment regimen at 5 mg/kg per day through IP injection. For the nilotinib + artesunate group, nilotinib was provided through OG and artesunate through IP injection. For bosutinib + artesunate group, both were provided through IP injections.

To measure organ edema, mice were injected intravenously with 200 μL of 1% Evans blue dye (Sigma Aldrich) through the retro-orbital plexus under anesthesia 45 minutes before euthanasia. Perfused brains and lungs were collected, and Evans blue dye was extracted and quantified by spectrophotometry as detailed in the supplemental Methods.

For histologic analysis, the brain and lungs were collected from infected or uninfected mice, treated or untreated with nilotinib or bosutinib on their own or coadministered with artesunate, on the seventh or eighth day after infection. Tissue collection, preparation, and analysis are detailed in the supplemental Methods.

All mice experiments were approved by the Seattle Children's Institutional Animal Care and Use Committee under protocol ACUC00649.

Statistical analysis

Statistical analysis was performed using Prism software (GraphPad Software Inc., version 8). Data are presented as mean ± standard deviation. A P value ≤.05 was considered statistically significant. Survival curves were analyzed using log-rank tests (Mantel Cox tests). For comparisons between multiple groups, the data were compared using analysis of variance. To assess the differences between groups and to adjust for multiple comparisons, the Dunnett test was used to compare all groups against a single group.

Results

Bosutinib and nilotinib attenuate thrombin-induced barrier disruption in HBMECs with different kinetics

Previously, we found that BCR-ABL drugs can variably alter thrombin-induced barrier disruption in HBMECs.[41] Here, we expanded on this study by comparing the 5 clinically approved BCR-ABL drugs. HBMECs were treated with 5 nM thrombin, and the barrier changes were evaluated using the xCELLigence system, which reports cell index as a proxy for barrier integrity. Thrombin induced an acute cell index drop with a maximum barrier disruption peak between 20 and 30 minutes after exposure, followed by recovery over the next 2 hours (Figure 1A). The KIs were added to HBMECs 7 minutes after thrombin treatment and barrier activity was evaluated by calculating the area under the curve for the cell index and then normalizing to the area under the curve for the DMSO vehicle control (Figure 1A). As before,[41] bosutinib was protective, imatinib was neutral, and dasatinib worsened thrombin-induced disruption. By comparison, nilotinib was mildly protective and ponatinib was weakly protective (Figure 1A).

To further investigate the mechanism(s) of drug action, we performed dose-titration experiments for bosutinib, nilotinib, and imatinib. In vivo, bosutinib achieves therapeutic plasma concentrations of 100 to 300 nM in humans as opposed to 1 to 2 μM for nilotinib in plasma.[47,48] Dose-response studies demonstrated that bosutinib was more effective at attenuating thrombin disruption than either nilotinib or imatinib across concentrations ranging from 30 nM to 2 μM (Figure 1B; supplemental Figure 1). The barrier-protective effects of nilotinib reached statistical significance only at higher concentrations (Figure 1B; supplemental Figure 1). Among the BCR-ABL inhibitors tested, bosutinib involved a 2-step mechanism with blunting of barrier disruption and expedited recovery (Figure 1B-C), conferring a V-shaped recovery slope. By comparison, nilotinib had a single-step mechanism of expediting barrier recovery (Figure 1B-C; supplemental Figure 1). We further investigated BCR-ABL drugs in cytokine storm–associated vascular injury using sequential tumor necrosis factor exposure, followed by thrombin-mediated barrier disruption. Interestingly, nilotinib treatment conferred enhanced barrier protection to thrombin challenge alone and was equally as effective as bosutinib, whereas imatinib showed no significant activity (supplemental Figure 1C). To visualize these effects, we conducted confocal microscopy analysis using immunofluorescent labeling of VE-cadherin, the major adherens junction protein, combined with phalloidin staining to label the actin cytoskeleton. Thrombin-treated HBMECs had substantial gaps in the endothelial monolayer at the 50-minute timepoint, which were associated with the loss of circumferential VE-cadherin and actin stress fibers (Figure 1C). Although actin stress fiber formation persisted across all drug treatments, bosutinib uniquely reduced thrombin-induced gap formation at 50 minutes, an effect not observed with nilotinib or imatinib (Figure 1C). Taken together, this analysis shows that bosutinib and nilotinib were the most protective against host proinflammatory mediators and that bosutinib exhibited faster barrier protective action than the other BCR-ABL drugs in thrombin-treated HBMECs.

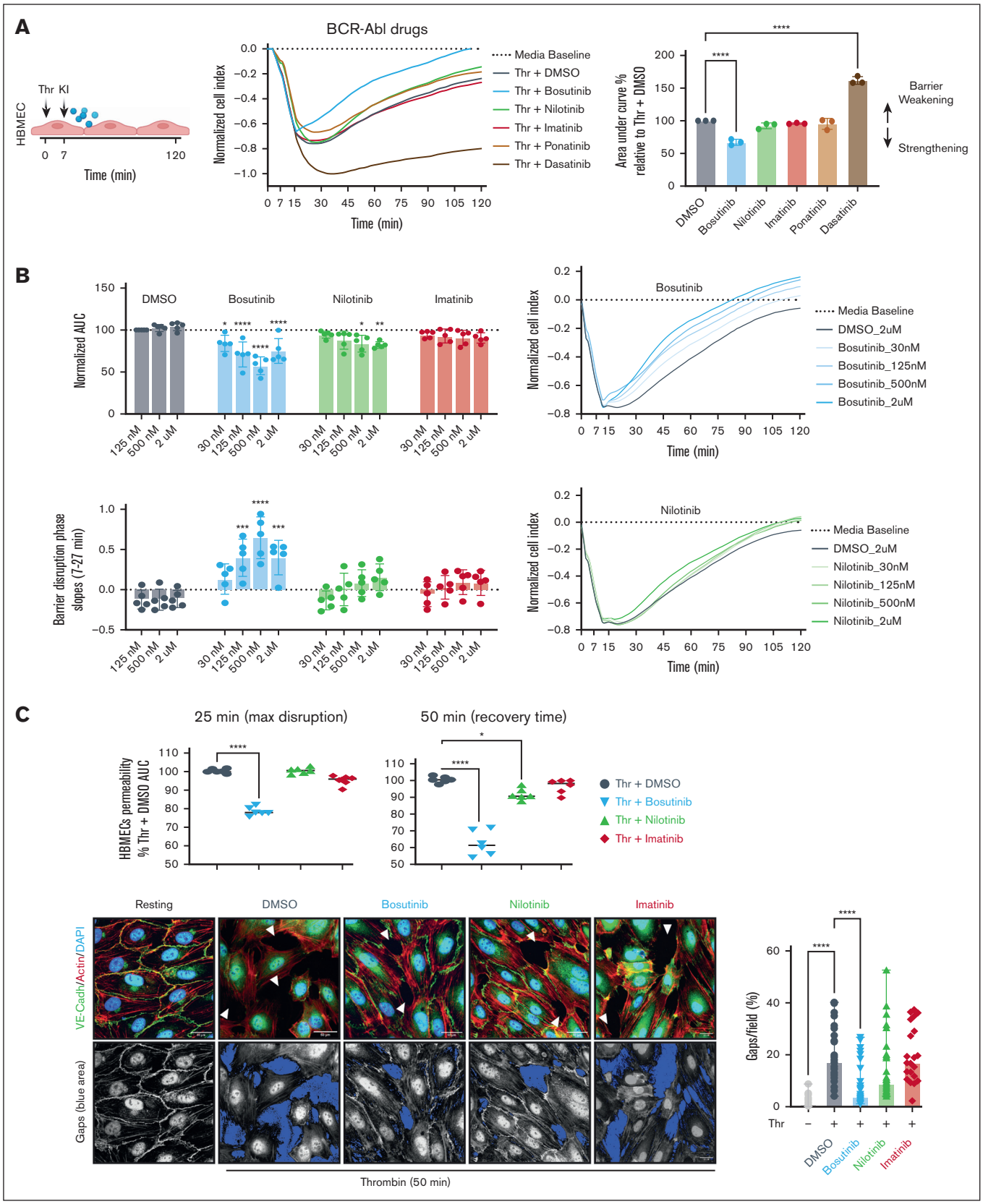

Figure 1. Bosutinib and nilotinib can attenuate Thr-induced barrier disruption in HBMECs. (A) Left, schematic overview. An xCELLigence assay was used to measure thrombin (Thr)-induced barrier disruption in an HBMEC monolayer. Traces were normalized to media control. KIs (0.5 μM) were added 7 minutes after Thr to assess barrier

Bosutinib attenuates phosphorylation of adherens junctions and focal adhesions during thrombin-induced endothelial gap formation

Phosphorylation of key junctional proteins, like VE-cadherin (Y685)[49-51] and the focal adhesion protein paxillin (Y118),[52,53] have been associated with endothelial barrier disruption. We investigated whether bosutinib, which inhibits both ABL and the c-Src kinases responsible for these phosphorylations (Figure 2A), is more effective than nilotinib and imatinib at reducing phosphorylation at these sites. We probed kinase phosphorylation during barrier disruption by western blotting, and the phosphoprotein levels were normalized to total protein levels. HBMECs were pretreated with thrombin for 7 minutes, followed by addition of the KIs. Thrombin induced a transient ~2.3-fold increase in VE-cadherin (Y685) phosphorylation, peaking at 20 to 30 minutes after thrombin exposure (Figure 2B-C). Paxillin (Y118) phosphorylation exhibited a slower onset but was sustained over 60 minutes (Figure 2B-C). Bosutinib (ABL + c-Src inhibitor)[54] substantially reduced thrombin-induced phosphorylation at both VE-cadherin (Y685) and paxillin (Y118), which coincided with its rapid barrier protective effect observed in the xCELLigence assay (Figure 2C). Conversely, nilotinib and imatinib, which inhibit ABL but not c-Src,[54] did not attenuate phosphorylation at either site (Figure 2B-C; supplemental Figure 2).

BCR-ABL drugs differ in attenuating parasite-induced permeability in primary HBMEC

To study BCR-ABL drugs against parasite inflammatory factors, we assessed bosutinib, nilotinib, and imatinib in a 2-cycle *P falciparum* growth inhibition assay (Figure 3A; supplemental Figure 3). All the KIs displayed nanomolar to micromolar range potency against asexual parasite growth (Figure 3B-C). Bosutinib and nilotinib prevented trophozoite progression, whereas imatinib targeted the late schizont stage (Figure 3C), consistent with previous findings that BCR-ABL drugs can kill *P falciparum* blood stage parasites and that imatinib inhibits IE rupture and the release of invasive merozoites.[35,36]

Because these drugs exhibited antiparasitic growth effects against blood-stage Pf-IEs, we first employed lysates of schizont-stage Pf-IEs (Pf-IE lysates) to investigate the potential protective effects of BCR-ABL drugs against Pf-IE–induced endothelial barrier disruption.[15] Consistent with previous findings,[55,56] Pf-IE lysates induced a mild and gradual decline in barrier integrity over several hours (cell index: Pf-IE lysate −0.3 maximum drop at 6 hours) when compared with control red blood cell lysate (Figure 4A; supplemental Figure 4). Among the BCR-ABL inhibitors, bosutinib demonstrated substantial efficacy in blunting Pf-IE lysate–induced barrier disruption, whereas nilotinib and imatinib showed no protective effect (Figure 4A). Temporal western blot analysis revealed that Pf-IE lysates triggered a transient ~2.3-fold increased phosphorylation of VE-cadherin (Y685) and a sustained ~4.5-fold increase in paxillin (Y118) phosphorylation (Figure 4B-C). Notably, bosutinib substantially attenuated phosphorylation at both sites, whereas nilotinib and imatinib did not (Figure 4B-C; supplemental Figure 4).

To simulate sequestered Pf-IEs, we used MACS-purified schizont-stage IT4var19-IEs (DC8-EPCR binder)[19] in co-culture with an HBMEC monolayer. After 1 hour of incubation, the KIs or DMSO vehicle control was added. This model similarly induced moderate and gradual barrier disruption (Figure 4D). Consistent with the lysate experiments, bosutinib significantly reduced schizont-IE–induced barrier disruption, whereas imatinib and nilotinib remained ineffective (Figure 4D).

In vivo efficacy of nilotinib and bosutinib in a mouse CM model

To assess the in vivo efficacy of BCR-ABL drugs, we used the mouse ECM model. Control PbANKA-infected C57BL/6 mice began to lose weight by day 5 after infection and experienced a decline in the 20-point RMCBS used to monitor infection[46] by days 6 or 7 (supplemental Figure 5). By day 7, ~50% of the mice reached the euthanasia cutoff (RMCBS score ≤5), which increased to 85% by day 8 and to 92% by day 9 (supplemental Figure 5). Hematoxylin and eosin–stained sections from mice with RMCBS scores (≤10) showed both brain pathology (brain hemorrhages and vascular congestion) and lung pathology (areas with alveolar edema, lung hemorrhage, congestion, cellular infiltration, and hyaline membrane; Figure 5A; supplemental Figures 6 and 7). Evans blue perfusion studies on day 7 after infection demonstrated 3 distinct phenotypes, namely (1) severe pulmonary edema with variable cerebral edema, (2) moderate cerebral edema with minimal pulmonary involvement, and (3) mild to moderate edema in both organs (Figure 5B). These findings indicate that a PbANKA infection induces complex multi-organ pathology.

Subsequently, we administered daily treatments of nilotinib, bosutinib, or imatinib to PbANKA-infected mice from days 4 to 7 after infection (early treatment regimen; Figure 5C). Nilotinib conferred the strongest protection (90%) when compared with bosutinib (25%) and imatinib (30%; Figure 5D). Although all the cohorts exhibited characteristic weight loss by day 4, nilotinib-treated mice recovered the most rapidly (supplemental Figure 8). Nilotinib most effectively suppressed parasitemia (Figure 5E) and reduced brain and lung edema (Figure 5F-G). Bosutinib-treated mice exhibited multiple day–delayed parasitemia suppression but had reduced organ edema by days 7 to 8 despite suboptimal parasite control (Figure 5F-G). Imatinib showed no effect on PbANKA parasitemia

Figure 1 (continued) protective activity. Right: the total change in the cell index is summarized as the area under the curve (AUC) quantification relative to that of DMSO treatment (100%). The data are presented as mean ± standard deviation (SD; n = 3, each done in duplicate). (B) Dose titration of bosutinib, nilotinib, and imatinib in the xCELLigence assay in Thr-treated HBMECs. The data are presented as mean ± SD (n = 5, each done in triplicate). (C) Top, quantification of Thr-induced barrier permeability at the maximum disruption time point (25 minutes) and at a mid-recovery time point (50 minutes), determined using xCELLigence assay. The data are presented as means ± SD (n = 3, each done in duplicate). Bottom left, representative confocal images of HBMECs under resting or Thr-activated conditions at 50 minutes in the presence or absence of KIs (0.5 μM). The fluorescence of VE-cadherin (green), phalloidin (red), and DAPI (blue) are shown. Gaps are indicated as white arrowheads. Bottom right panel: the highlighted blue areas represent gaps in the monolayer. ImageJ quantification showing the percentage intercellular gaps per field, calculated from 8 uniformly sampled fields (n = 3). A 1-way analysis of variance (ANOVA), followed by Dunnett multiple comparison test, was used to analyze the data. *$P < .05$; ****$P < .0001$.

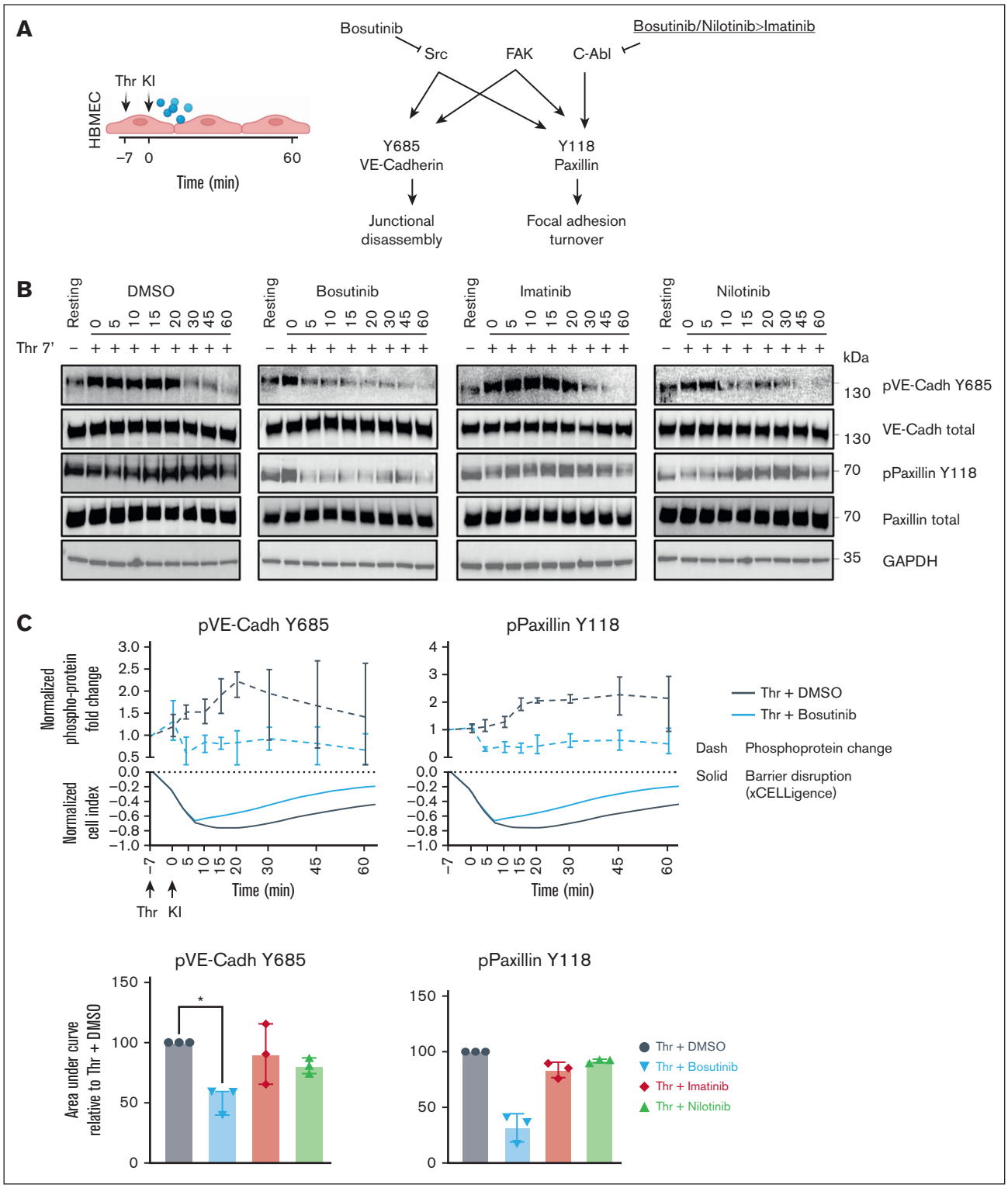

Figure 2. Bosutinib attenuates phosphorylation of adherens junctions and focal adhesions during Thr-induced endothelial barrier disruption. (A) A schematic overview of the target selectivity of BCR-ABL drugs against 3 kinases that phosphorylate VE-cadherin (Y685) and paxillin (Y118). (B) Thrombin (Thr)-induced temporal phosphorylation kinetics of VE-cadherin (Y685) and paxillin (Y118) were probed using immunoblotting, along with their respective total proteins. GAPDH was used as a loading control (n = 3). (C) Upper panel, Thr-induced fold change of the indicated phosphoprotein in the presence of DMSO vehicle control or bosutinib is plotted above the respective xCELLigence traces. ImageJ quantification of phosphoproteins levels in panel B was adjusted to the total protein amounts, and fold change was calculated by normalizing to the resting state (nontreated, media only). The data are presented as means ± SD (n = 3). Lower panel, quantification of the KI effect on phosphorylation (total protein normalized) in the presence of KIs or DMSO control (100%). The bars represent the median AUC ± SD (n = 3). A 1-way ANOVA, followed by Dunnett multiple comparison test, was used to analyze the data. *$P < .05$. FAK, focal adhesion kinase; GAPDH, glyceraldehyde-3-phosphate dehydrogenase; pVE-Cadh, protein VE-cadherin.

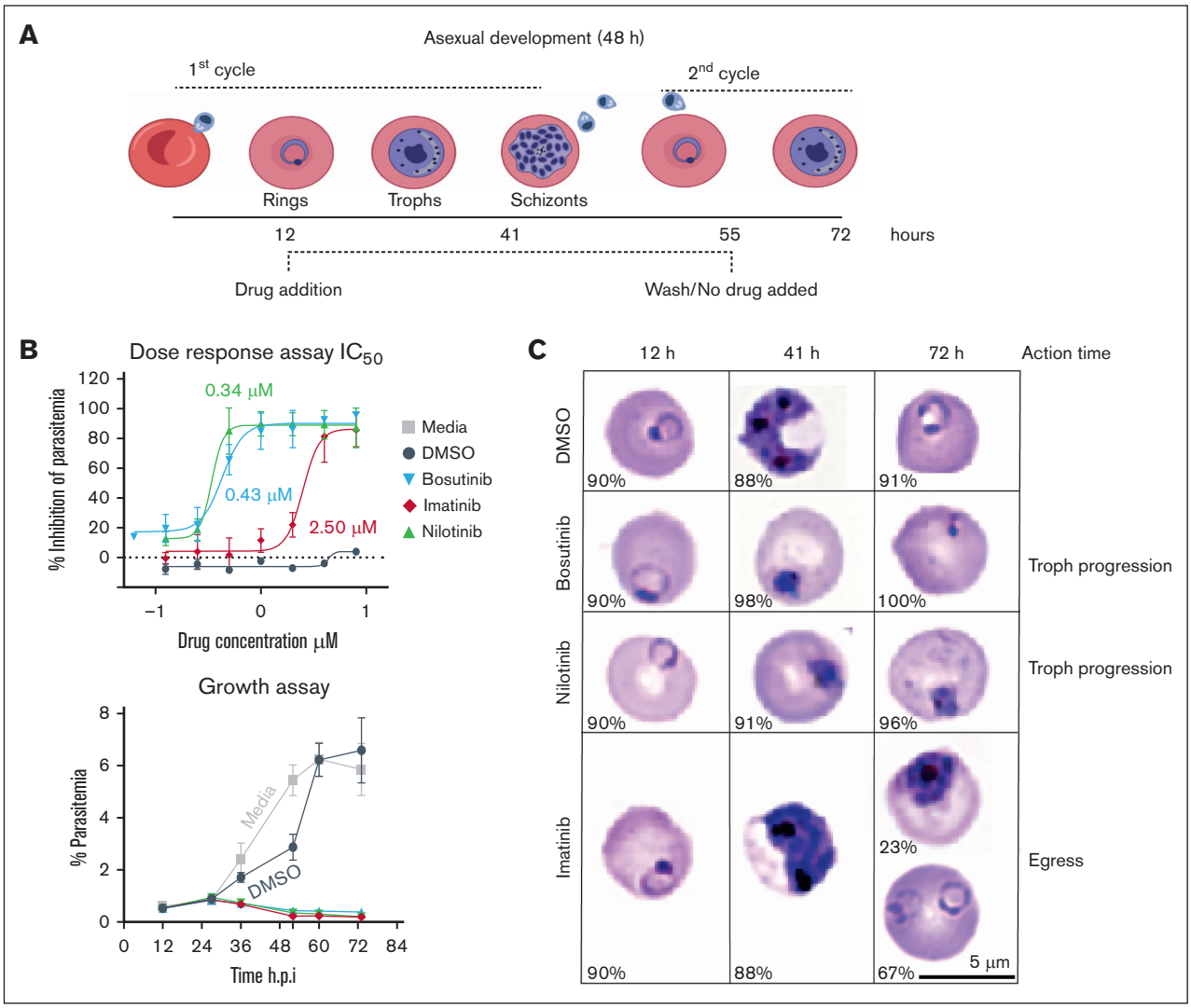

Figure 3. BCR-ABL drugs suppress *P falciparum* growth in RBCs. (A) Schematic of the 2-cycle *P falciparum* blood stage growth inhibition assay. (B) Upper panel, 2-fold dose-response curve ranging from 0.1 to 8 µM, followed by a media wash at 55 hours. Parasitemia was measured using SYBR staining with flow cytometry, which was performed at 72 hours. The half-maximal inhibitory concentrations (IC_{50}) of the drugs are indicated. Lower panel, *P falciparum* asexual intraerythrocytic growth assay. At the ring stage (~12 h after invasion), media only treatment or treatment with 4 µM KIs or DMSO (vehicle) was applied. The parasites were grown for 2 consecutive growth cycles and the percentage parasitemia was determined using SYBR staining with flow cytometry every 12 hours after infection. The data are presented as means ± SD (n = 3). (C) Representative bright field images of Giemsa-stained blood smears for parasite maturation during drug assay. The percentage of the representative parasite stage is shown at the bottom left corner of each Giemsa-stained image for the respective time point and treatment condition. Scale bar = 5 µm. RBCs, red blood cells.

(Figure 5E). The reduced half-lives of BCR-ABL inhibitors in C57BL/6 mice (1-3 hours) as opposed to in humans may account for their reduced antiparasitic efficacy.[57] These data demonstrate that nilotinib and bosutinib reduce brain and lung edema in the early-intervention ECM model through distinct mechanisms of action.

Nilotinib rescues mice and reduces brain and lung pathology in a late-stage treatment regimen

In a clinical setting, BCR-ABL drugs would be used in combination with the existing front-line antimalaria treatment artesunate. To explore BCR-ABL drugs in this context, mice were administered nilotinib or bosutinib on days 6 to 10 after infection (late-stage treatment; Figure 6A), coinciding with initial RMCBS score deterioration. Four experimental mice cohorts were compared, namely (1) infection control, (2) subtherapeutic dose of artesunate alone (5 mg/kg per day), (3) nilotinib or bosutinib alone, and (4) nilotinib or bosutinib as adjunctive therapy with artesunate (nilotinib or bosutinib + artesunate). Nilotinib conferred stronger protection than bosutinib as a monotherapy (44% vs 16%; Figure 6B; supplemental Figure 9). In addition, some mice in the bosutinib treatment group experienced fatal internal bleeding and suddenly died without a decline in the RMCBS score, prompting subsequent analyses to focus exclusively on nilotinib. Although individual nilotinib or artesunate treatments each conferred ~44% protection, combination therapy enhanced survival to 78% (Figure 6B). The

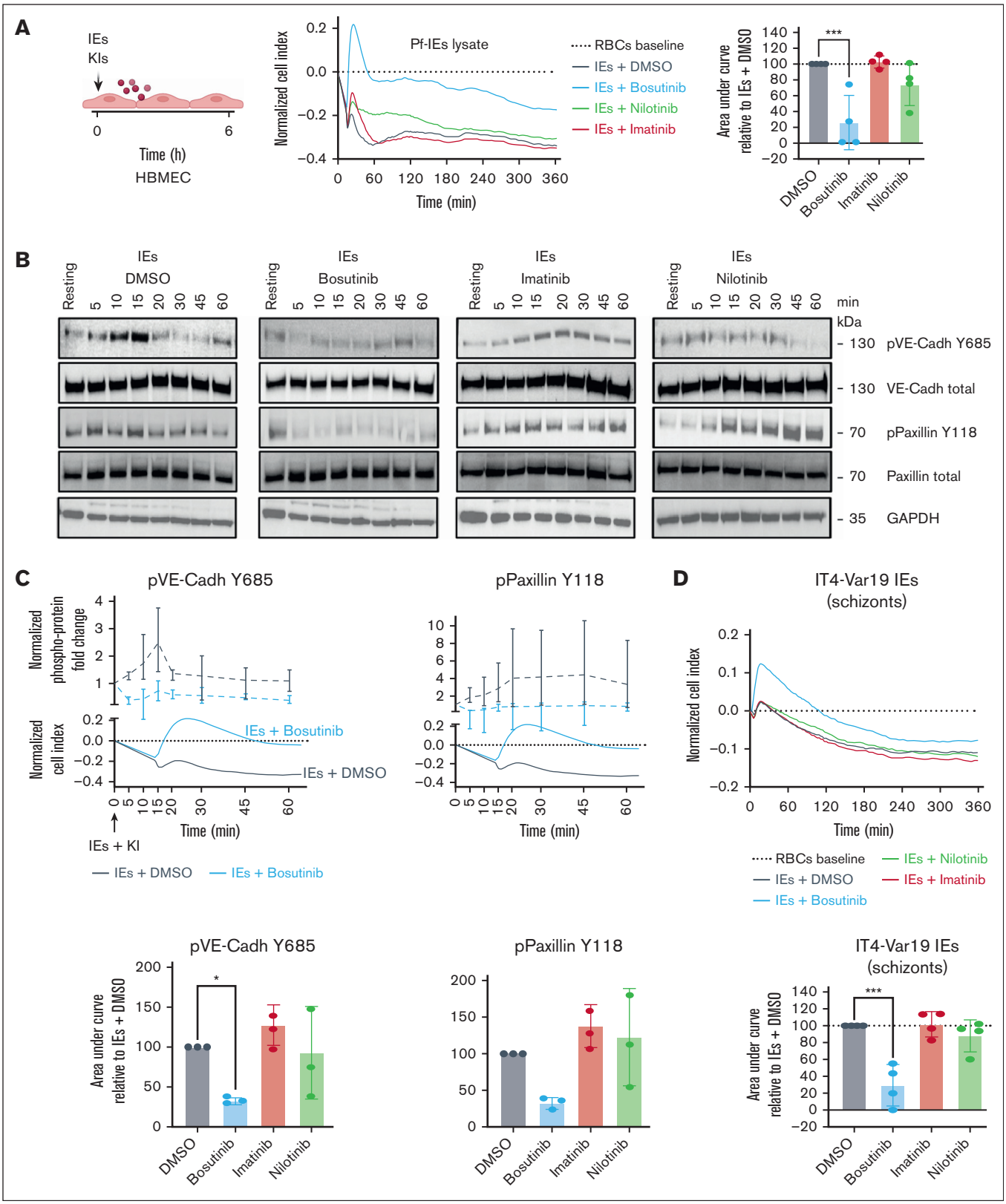

Figure 4. Bosutinib can attenuate parasite-induced barrier disruption in HBMECs. (A) Schematic overview of the parasite-permeability assay. Representative xCELLigence recordings of HBMECs treated with lysates from 3D7 Pf-IEs. The traces were normalized to that of uninfected RBC lysates. KIs (0.5 μM) were added at the same time as the parasite lysate. Right, total change in cell index is summarized as the AUC relative to that of DMSO (100%). The data are presented as the mean ± SD (n = 4, done in duplicate). *$P < .05$ determined using a 1-way ANOVA, followed by Dunnett multiple comparison test (compared with the DMSO/Pf-IEs lysate group). (B) 3D7 Pf-IE

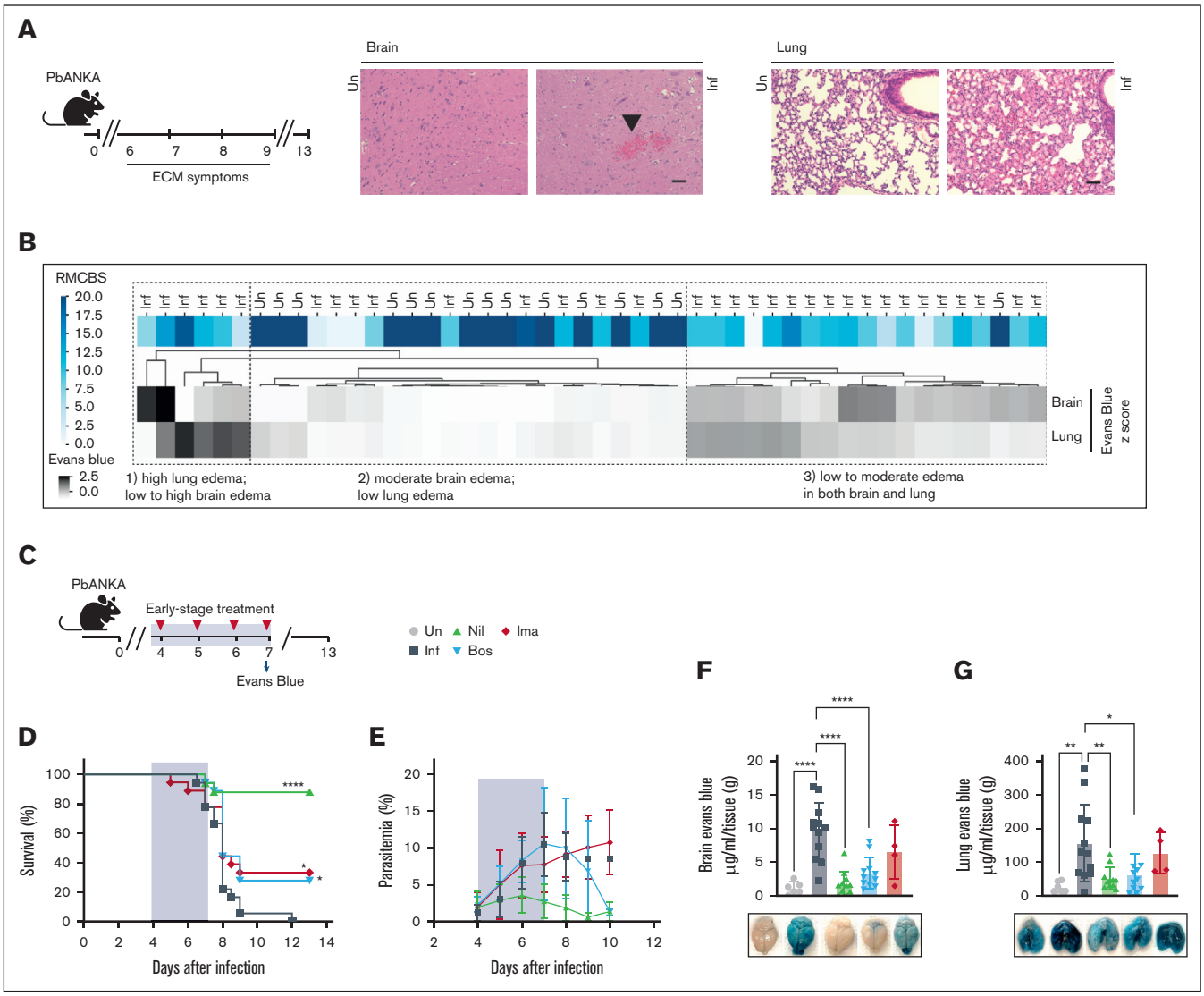

Figure 5. BCR-ABL drugs attenuate ECM pathology and protect mice when provided before ECM symptoms develop. (A) Schematic overview of the ECM assay. Representative hematoxylin and eosin images of the brain and lung of uninfected (Un) and PbANKA-infected (Inf) mice euthanized on day 7 after infection with RMCBS score <8 (20×; scale bar = 50 µm). The arrowhead indicates brain hemorrhage. (B) Unsupervised hierarchical cluster map of brain and lung edema measured by Evans blue dye on day 7 after infection (gray scale) in comparison with the RMCBS clinical score (blue scale). (C) Schematic overview of the early-infection drug regimen (days 4 to 7). (D) Survival curves (mice were euthanized at an RMCBS score of ≤5; n = 18 Inf; 17 nilotinib [Nil]; 18 bosutinib [Bos]; 18 imatinib [Ima]). *$P < .05$; ****$P < .0001$ determined using a log-rank test (Mantel Cox test) in comparison with the Inf group. (E) Parasitemia curves (n = 18 Inf; 17 Nil; 18 Bos; 18 Ima). (F) Brain edema measured by Evans blue assay on day 7 after infection (n = 6 Un; 12 Inf; 11 Nil; 11 Bos; 4 Ima). ****$P < .0001$ determined using 1-way ANOVA, followed by Dunnett multiple comparison test (compared with the Inf group). (G) Lung edema measured by Evans blue assay on day 7 after infection (n = 6 Un; 12 Inf; 11 Nil; 11 Bos; 4 Ima). *$P < .05$; **$P < .01$ determined using a 1-way ANOVA, followed by Dunnett multiple comparison test (compared with the Inf group).

Figure 4 (continued) lysate–induced phosphorylation of VE-cadherin (Y685) and paxillin (Y118) were probed using immunoblotting, along with their respective total proteins. GAPDH was used as a loading control. The western blot images are representative of 3 independent biologic replicates. (C) Upper panel, the 3D7 Pf lysate–induced fold change of the indicated phosphoproteins levels, adjusted to the total protein amounts (dashed lines), is plotted above the Pf lysate-induced change in the cell index (solid lines), measured using the xCELLigence platform in panel (A). Fold change was calculated by normalizing the data against the data of the resting state (nontreated, media only). Lower panel, The AUC was calculated for the temporal phosphoprotein kinetics (total protein normalized) in the presence of KIs or for the DMSO control (100%). Bars represent the mean AUC ± SD (n = 3). ***$P < .001$; *$P < .05$ determined using 1-way ANOVA, followed by Dunnett multiple comparison test (compared with DMSO control). (D) Upper panel, representative recording of xCELLigence barrier response to schizont-stage IT4var19-IEs (after normalization to uninfected RBCs). DMSO or KIs (0.5 µM) were added after 1 hour of co-culture of purified schizont-stage IEs or RBCs with HBMECs. Lower panel, quantification of barrier protective activity of KIs against schizont-induced barrier disruption. The data are presented as mean ± SD (n = 4, each done in triplicate). ***$P < .001$ determined using a 1-way ANOVA, followed by Dunnett multiple comparison test (compared with the DMSO/Pf-IEs group). GAPDH, glyceraldehyde-3-phosphate dehydrogenase; pVE-Cadh, protein VE-cadherin; RBCs, red blood cells.

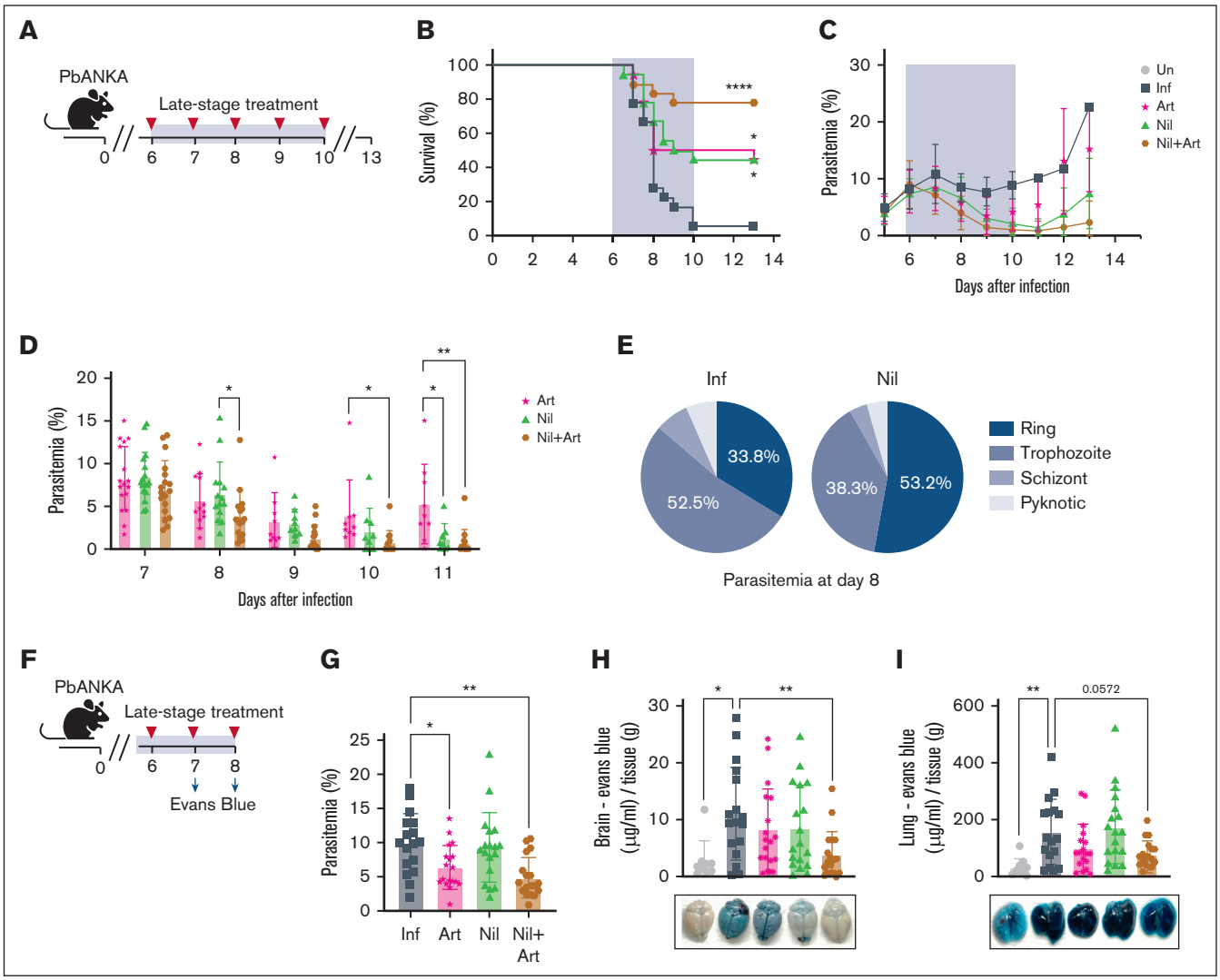

Figure 6. Coadministration of nilotinib with artesunate increased survival and decreased brain edema. (A) Schematic overview of the late-stage treatment regimen (days 6-10) as highlighted by the gray box. (B) Survival curves (mice were euthanized at an RMCBS score ≤ 5; n = 18 per group. *$P < .05$; **** $P < .0001$ analyzed using log-rank tests [Mantel Cox tests] in comparison with the infected group). (C) Parasitemia curves (n = 18 per group). (D) Parasitemia in individual mice on days 7 to 11 after infection. *$P < .05$; **$P < .01$ determined using 2-way ANOVA, followed by Tukey multiple comparison test. (E) Giemsa-stained blood smears were used to determine the parasite life stages on day 8 after infection in the no treatment and nilotinib-treated PbANKA-infected mice. (F) Schematic overview of Evans blue dye assay conducted on day 7 or 8. (G) Parasitemia measured on the day of Evans blue dye assay (n = 9 Un; 17 Inf; 18 Art; 18 Nil+Art). * $P < .05$; **$P < .01$ determined using 1-way ANOVA, followed by Dunnett multiple comparison test (compared with the infected group). (H) Brain edema measured by Evans blue assay on day 7 or 8 after infection (n = 9 Un; 17 inf; 18 Art; 18 Nil+Art). *$P < .05$; **$P < .01$ determined using 1-way ANOVA, followed by Dunnett multiple comparison test (compared with the infected group). (I) Lung edema measured by Evans blue assay on day 7 or 8 after infection (n = 9 Un; 17 Inf; 18 Art; 18 Nil+Art). **$P < .01$ determined using 1-way ANOVA, followed by Dunnett multiple comparison test (compared with the infected group). Art, artesunate.

combination treatment cohort of nilotinib + artesunate exhibited accelerated parasite clearance (Figure 6C-E). To investigate the effect of BCR-ABL drugs on organ edema, we performed an Evans blue perfusion assay on day 7 or day 8 after infection, concurrent with significant RMCBS score decline (≤ 5) in control mice (Figure 6F; supplemental Figure 8). At assessment, both artesunate and the nilotinib + artesunate treatment groups had lower parasitemia than the nilotinib alone or infection control mice (Figure 6G). The combined nilotinib + artesunate treatment reduced brain edema ($P = .01$) and showed a trend toward reduced lung edema that did not achieve statistical significance ($P = .0572$; Figure 6H-I).

Histopathologic evaluation of vascular pathology was performed on day 8 after infection (Figure 7A). Despite comparable parasitemia between the nilotinib and artesunate cohorts (Figure 7B), nilotinib treatment significantly reduced brain and lung hemorrhages (Figure 7C-G). In addition, the nilotinib + artesunate group

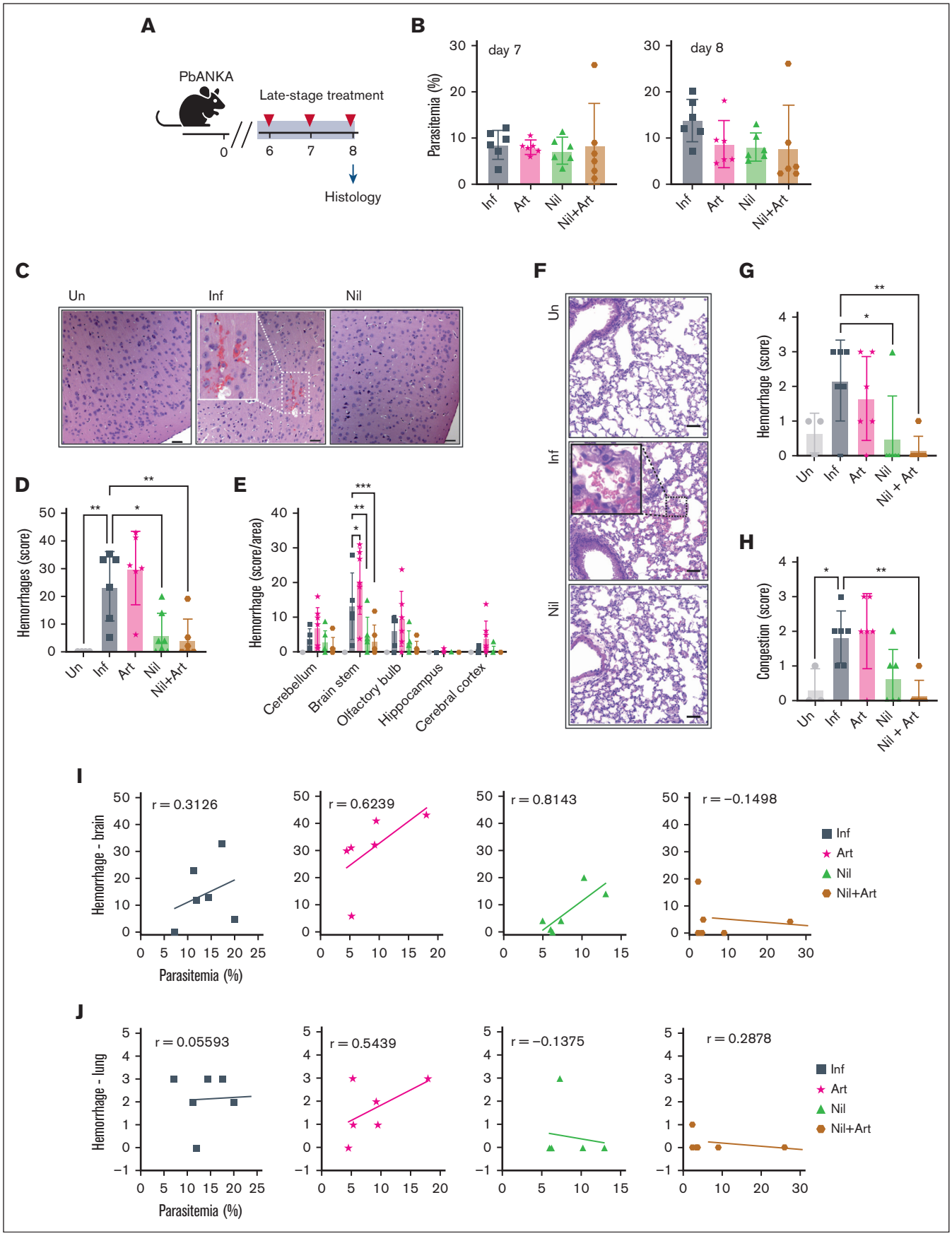
A
PbANKA
Late-stage treatment
0
6
7
8
Histology
B
day 7
day 8
Parasitemia (%)
Inf
Art
Nil
Nil+Art
C
Un
Inf
Nil
D
Hemorrhages (score)
E
Hemorrhage (score/area)
Cerebellum
Brain stem
Olfactory bulb
Hippocampus
Cerebral cortex
F
Un
Inf
Nil
G
Hemorrhage (score)
Nil + Art
H
Congestion (score)
I
Hemorrhage - brain
Parasitemia (%)
r = 0.3126
r = 0.6239
r = 0.8143
r = −0.1498
J
Hemorrhage - lung
r = 0.05593
r = 0.5439
r = −0.1375
r = 0.2878

Figure 7.

exhibited reduced lung congestion (Figure 7H). The vascular protective effect of nilotinib against hemorrhages was particularly prominent in the brain stem (Figure 7E). Nilotinib-treated mice had fewer brain and lung hemorrhages than the artesunate or control-infected mice at both low and high levels of parasitemia (Figure 7I-J). The combination therapy nilotinib + artesunate group exhibited minimal brain and lung hemorrhages when compared with the other treatment groups (Figure 7I-J). Collectively, these findings demonstrate nilotinib's ability to attenuate brain and lung hemorrhages, both as a monotherapy or when coadministered with an antimalaria drug.

Discussion

Our research corroborates previous findings that BCR-ABL drugs inhibit blood stage *P falciparum* growth[34-36] with nilotinib and bosutinib preventing trophozoite progression and imatinib targeting late blood-stage parasites. Because coadministration of imatinib with antimalaria drugs accelerated parasite clearance and fever resolution in Vietnamese patients with uncomplicated malaria,[37] we evaluated the potential anti-inflammatory properties of BCR-ABL drugs in severe malaria models.

Sequestration is central to *P falciparum* CM pathogenesis,[9,58] triggering both systemic inflammation and localized cerebrovascular inflammation from both pathogen-associated molecular patterns, such as parasite histones[11,12] and *P falciparum* histidine rich protein 2,[14] and malaria damage–associated molecular patterns, including heme,[59,60] uric acid,[61,62] and extracellular vesicles.[63] Although Pf-IEs can promote the disruption of brain endothelial cell monolayers,[15] the underlying molecular mechanisms remain poorly understood. By using primary HBMECs, we observed that thrombin induced an acute, reversible barrier disruption and that Pf-IEs elicited a mild and gradual alteration in barrier phenotype. Among the 5 BCR-ABL drugs, bosutinib and nilotinib were the most effective at protecting HBMEC barrier integrity against tumor necrosis factor and thrombin, which are 2 key host inflammatory mediators in human CM. Our analysis showed that bosutinib exhibited a distinctive 2-step mechanism by both blunting thrombin disruption and accelerating barrier recovery. Conversely, nilotinib primarily hastened barrier recovery. Furthermore, only bosutinib proved effective against Pf-IE–induced barrier disruption, suggesting distinct mechanistic pathways. We found that bosutinib was uniquely able to prevent the phosphorylation of ABL- and c-Src–dependent sites in VE-cadherin and paxillin[49,51,52] that was induced by both thrombin and parasite stimuli, consistent with a role of the Src-family of kinases in parasite-induced barrier disruption.[64] Bosutinib's protective mechanism extended to strengthening endothelial junctions and focal adhesions in thrombin-treated human umbilical vein endothelial cells via a mitogen-activated protein 4 kinase 4–dependent pathway.[38] Taken together, these findings indicate commonalities in bosutinib's protective effects against different permeability mediators through interference with kinase regulators of the adherens junctions and focal adhesions. In contrast, nilotinib showed limited impact on barrier disruption and primarily facilitated barrier recovery through undefined molecular mechanisms. The remaining BCR-ABL inhibitors displayed either minimal effects (imatinib and ponatinib) or exacerbated barrier disruption (dasatinib), likely reflecting their distinct polypharmacologic profiles.[41,54] Overall, these findings highlight the diverse phenotypes of BCR-ABL drugs on both endothelial barrier function and in blood-stage *P falciparum* killing assays, underscoring the complexity of their interactions with host-parasite systems.

Given the absence of animal models of *P falciparum* CM, we used the mouse ECM model to evaluate in vivo drug efficacy. It should be noted that *P berghei* parasites lack the *P falciparum* erythrocyte membrane protein 1 (PfEMP1) cytoadhesion protein family, which leads to reduced accumulation of IEs in the mouse brain.[65,66] Despite this limitation, the mouse ECM model has been extensively employed to investigate adjunctive therapies aimed at counteracting inflammation in CM.[67-72] In mice, nilotinib demonstrated superior efficacy over bosutinib and imatinib, primarily attributable to nilotinib's substantially greater effectiveness in controlling parasitemia. Nevertheless, bosutinib reduced brain and lung edema when administered in an early intervention regimen despite having no impact on parasitemia. However, when administered in a late infection treatment regimen, some mice experienced adverse bleeding side effects, which align with the known bosutinib-associated effects, including thrombocytopenia and platelet function effects.[73,74] These findings warrant circumspection in the repurposing of bosutinib for severe malaria treatment. Future work is needed to understand what drives these different outcomes and whether an optimal dose regimen can be established in the ECM model to ensure both safety and efficacy in potential clinical applications. Although mice treated with nilotinib and artesunate had equivalent levels of parasitemia, nilotinib led to less brain hemorrhages and reduced vascular congestion, including fewer hemorrhages within the brain stem, a site of extensive vascular leak and neuronal apoptosis in the ECM model.[75] This finding is particularly significant given that petechial brain hemorrhages are a characteristic pathologic feature observed in two-thirds of fatal pediatric CM cases.[9,28] The in vivo mechanism(s) of action for nilotinib is likely to be multifaceted and intricate. CD8 T cells play a critical role in fatal brain edema in the mouse ECM model.[75-79] Beyond parasitemia control and barrier restorative activity in a primary brain endothelial cell in vitro model, nilotinib can hamper in vitro CD8 T cell proliferation and effector function[80,81] and targets a host tyrosine kinase receptor implicated in endothelial

Figure 7. Nilotinib reduces brain and lung hemorrhages in late-stage treatment intervention. (A) Schematic overview of the histology study conducted on day 8 after infection. (B) Parasitemia in mice on day 7 and 8 after infection (n = 6 mice per group). (C) Representative hematoxylin and eosin (H&E)–stained brain sections of uninfected (Un), infected (Inf), and nilotinib (Nil)-treated mice. Hemorrhage (white dashed box) in the cerebral cortex area on day 8 after infection (magnification ×10; scale bar = 100 μm; magnification ~×3.6, boxed inset). (D) Total brain hemorrhage score. (E) Individual brain area hemorrhage score. (F) Representative H&E lung sections (magnification ×20; scale bar = 50 μm) showing hemorrhage area (black dashed box; magnification ~×4, boxed inset). Lungs were collected on day 8 after infection. (G) Lung hemorrhage score. (H) Lung congestion score. (I) Correlation of parasitemia and brain hemorrhage score. (J) Correlation of parasitemia and lung hemorrhage score. A 1-way ANOVA, followed by Dunnett multiple comparisons test (compared with the infected group) was used to analyze the data. *$P < .05$; **$P < .01$; ***$P < .01$.

barrier integrity in the ECM model.[42] Nilotinib's potential to simultaneously influence multiple pathophysiological pathways suggest that it may represent a promising therapeutic approach for severe malaria. Further investigations are needed to delineate the in vivo mechanism(s) of action of nilotinib in the mouse ECM model.

Our study presents both strengths and limitations. A notable strength is the use of both a human in vitro brain endothelial model and the mouse ECM model, providing the evaluation of these drugs in a more complex environment. However, the ECM model, although valuable, does not perfectly replicate the human pathophysiology, especially for studying the Pf-IE driven inflammatory processes that are unique to human CM.[2] Consequently, the extrapolation of our murine findings to human scenarios has limitations. Further research is necessary to elucidate the pharmacokinetics and safety profiles of BCR-ABL drugs in the context of mild human malaria infections[37] and as candidate adjunctive therapies for pediatric CM.[82] Likewise, subsequent investigations in the murine ECM model are warranted to discern whether nilotinib's protective effect is primarily attributable to parasitemia control or potentially mediated by other anti-inflammatory mechanisms that may have translational relevance to human disease. In conclusion, these findings have significant implications for the repurposing of BCR-ABL drugs in malaria treatment and, simultaneously, may offer novel avenues to combat emerging drug-resistant parasites[83] and mitigate the adverse effects of inflammation in CM.

Acknowledgments

The authors thank Corey Layzer for technical assistance, the University of Washington histology core for histology preparations and sectioning, and Tracey J. Lamb (University of Utah) for providing the *P berghei* ANKA parasites used in the experiments. Illustrative images were created with BioRender.com.

This work was funded by the National Institutes of Health grant RO1 AI48802 (J.D.S. and A.K.).

Authorship

Contribution: L.S.O., P.B., A.K., and J.D.S. conceptualized the study; L.S.O., P.B., V.I.P., L.W., R.J.R.X.F., and S.E. contributed to the methodology; L.S.O., P.B., and V.I.P. performed the investigation; A.K. and J.D.S. supervised the study; L.S.O., P.B., and J.D.S. wrote the original draft; and all the authors wrote and edited the manuscript.

Conflict-of-interest disclosure: The authors declare no competing financial interests.

ORCID profiles: L.S.O., 0000-0003-1153-9987; P.B., 0000-0002-8751-1369; R.J.R.X.F., 0009-0009-6743-6865; L.W., 0000-0002-1825-8718; S.E., 0000-0001-6094-9750; A.K., 0000-0001-5721-258X; J.D.S., 0000-0002-7915-6360.

Correspondence: Joseph D. Smith, Center for Global Infectious Disease Research, Seattle Children's Research Institute, 1916 Boren Ave, Seattle, WA 98101; email: joe.smith@seattlechildrens.org.

References

1. Lee WL, Slutsky AS. Sepsis and endothelial permeability. *N Engl J Med*. 2010;363(7):689-691.
2. Miller LH, Ackerman HC, Su XZ, Wellems TE. Malaria biology and disease pathogenesis: insights for new treatments. *Nat Med*. 2013;19(2):156-167.
3. Weisberg E, Parent A, Yang PL, et al. Repurposing of kinase inhibitors for treatment of COVID-19. *Pharm Res*. 2020;37(9):167.
4. *World Malaria Report 2022*. Global Malaria Programme; 2022.
5. Idro R, Kakooza-Mwesige A, Asea B, et al. Cerebral malaria is associated with long-term mental health disorders: a cross sectional survey of a long-term cohort. *Malar J*. 2016;15:184.
6. Langfitt JT, McDermott MP, Brim R, et al. Neurodevelopmental impairments 1 year after cerebral malaria. *Pediatrics*. 2019;143(2):e20181026.
7. Dondorp AM, Fanello CI, Hendriksen IC, et al. Artesunate versus quinine in the treatment of severe falciparum malaria in African children (AQUAMAT): an open-label, randomised trial. *Lancet*. 2010;376(9753):1647-1657.
8. MacPherson GG, Warrell MJ, White NJ, Looareesuwan S, Warrell DA. Human cerebral malaria. A quantitative ultrastructural analysis of parasitized erythrocyte sequestration. *Am J Pathol*. 1985;119(3):385-401.
9. Taylor TE, Fu WJ, Carr RA, et al. Differentiating the pathologies of cerebral malaria by postmortem parasite counts. *Nat Med*. 2004;10(2):143-145.
10. Seydel KB, Kampondeni SD, Valim C, et al. Brain swelling and death in children with cerebral malaria. *N Engl J Med*. 2015;372(12):1126-1137.
11. Gillrie MR, Lee K, Gowda DC, et al. Plasmodium falciparum histones induce endothelial proinflammatory response and barrier dysfunction. *Am J Pathol*. 2012;180(3):1028-1039.
12. Moxon CA, Alhamdi Y, Storm J, et al. Parasite histones are toxic to brain endothelium and link blood barrier breakdown and thrombosis in cerebral malaria. *Blood Adv*. 2020;4(13):2851-2864.
13. Nguyen ST, Du D, Wychrij D, et al. Histidine-rich protein II nanoparticle delivery of heme iron load drives endothelial inflammation in cerebral malaria. *Proc Natl Acad Sci U S A*. 2023;120(26):e2306318120.
14. Pal P, Daniels BP, Oskman A, Diamond MS, Klein RS, Goldberg DE. Plasmodium falciparum histidine-rich protein II compromises brain endothelial barriers and may promote cerebral malaria pathogenesis. *mBio*. 2016;7(3):e00617-16.
15. Tripathi AK, Sullivan DJ, Stins MF. Plasmodium falciparum-infected erythrocytes decrease the integrity of human blood-brain barrier endothelial cell monolayers. *J Infect Dis*. 2007;195(7):942-950.

16. Moxon CA, Wassmer SC, Milner DA Jr, et al. Loss of endothelial protein C receptors links coagulation and inflammation to parasite sequestration in cerebral malaria in African children. *Blood*. 2013;122(5):842-851.
17. Gazzinelli RT, Kalantari P, Fitzgerald KA, Golenbock DT. Innate sensing of malaria parasites. *Nat Rev Immunol*. 2014;14(11):744-757.
18. Moxon CA, Gibbins MP, McGuinness D, Milner DA Jr, Marti M. New insights into malaria pathogenesis. *Annu Rev Pathol*. 2020;15:315-343.
19. Avril M, Tripathi AK, Brazier AJ, et al. A restricted subset of var genes mediates adherence of Plasmodium falciparum-infected erythrocytes to brain endothelial cells. *Proc Natl Acad Sci U S A*. 2012;109(26):E1782-E1790.
20. Bernabeu M, Gunnarsson C, Vishnyakova M, et al. Binding heterogeneity of Plasmodium falciparum to engineered 3D brain microvessels is mediated by EPCR and ICAM-1. *mBio*. 2019;10(3):e00420-19.
21. Kessler A, Dankwa S, Bernabeu M, et al. Linking EPCR-binding PfEMP1 to brain swelling in pediatric cerebral malaria. *Cell Host Microbe*. 2017;22(5):601-614.e5.
22. Lennartz F, Adams Y, Bengtsson A, et al. Structure-guided identification of a family of dual receptor-binding PfEMP1 that is associated with cerebral malaria. *Cell Host Microbe*. 2017;21(3):403-414.
23. Storm J, Jespersen JS, Seydel KB, et al. Cerebral malaria is associated with differential cytoadherence to brain endothelial cells. *EMBO Mol Med*. 2019;11(2):e9164.
24. Turner L, Lavstsen T, Berger SS, et al. Severe malaria is associated with parasite binding to endothelial protein C receptor. *Nature*. 2013;498(7455):502-505.
25. Bernabeu M, Smith JD. EPCR and malaria severity: the center of a perfect storm. *Trends Parasitol*. 2017;33(4):295-308.
26. Gillrie MR, Avril M, Brazier AJ, et al. Diverse functional outcomes of Plasmodium falciparum ligation of EPCR: potential implications for malarial pathogenesis. *Cell Microbiol*. 2015;17(12):1883-1899.
27. Petersen JEV, Bouwens EAM, Tamayo I, et al. Protein C system defects inflicted by the malaria parasite protein PfEMP1 can be overcome by a soluble EPCR variant. *Thromb Haemost*. 2015;114(5):1038-1048.
28. Dorovini-Zis K, Schmidt K, Huynh H, et al. The neuropathology of fatal cerebral malaria in Malawian children. *Am J Pathol*. 2011;178(5):2146-2158.
29. Gillrie MR, Renaux B, Russell-Goldman E, et al. Thrombin cleavage of Plasmodium falciparum erythrocyte membrane protein 1 inhibits cytoadherence. *mBio*. 2016;7(5):e01120-16.
30. Glennon EKK, Dankwa S, Smith JD, Kaushansky A. Opportunities for host-targeted therapies for malaria. *Trends Parasitol*. 2018;34(10):843-860.
31. Varo R, Crowley VM, Sitoe A, et al. Adjunctive therapy for severe malaria: a review and critical appraisal. *Malar J*. 2018;17(1):47.
32. Wei L, Adderley J, Leroy D, et al. Host-directed therapy, an untapped opportunity for antimalarial intervention. *Cell Rep Med*. 2021;2(10):100423.
33. Rossari F, Minutolo F, Orciuolo E. Past, present, and future of Bcr-Abl inhibitors: from chemical development to clinical efficacy. *J Hematol Oncol*. 2018;11(1):84.
34. de Sousa ACC, Maepa K, Combrinck JM, Egan TJ. Lapatinib, nilotinib and lomitapide inhibit haemozoin formation in malaria parasites. *Molecules*. 2020;25(7):1571.
35. Kesely KR, Pantaleo A, Turrini FM, Olupot-Olupot P, Low PS. Inhibition of an erythrocyte tyrosine kinase with imatinib prevents Plasmodium falciparum egress and terminates parasitemia. *PLoS One*. 2016;11(10):e0164895.
36. Pantaleo A, Kesely KR, Pau MC, et al. Syk inhibitors interfere with erythrocyte membrane modification during P falciparum growth and suppress parasite egress. *Blood*. 2017;130(8):1031-1040.
37. Chien HD, Pantaleo A, Kesely KR, et al. Imatinib augments standard malaria combination therapy without added toxicity. *J Exp Med*. 2021;218(10):e20210724.
38. Botros L, Pronk MCA, Juschten J, et al. Bosutinib prevents vascular leakage by reducing focal adhesion turnover and reinforcing junctional integrity. *J Cell Sci*. 2020;133(9):jcs240077.
39. Rizzo AN, Aman J, van Nieuw Amerongen GP, Dudek SM. Targeting Abl kinases to regulate vascular leak during sepsis and acute respiratory distress syndrome. *Arterioscler Thromb Vasc Biol*. 2015;35(5):1071-1079.
40. Rizzo AN, Sammani S, Esquinca AE, et al. Imatinib attenuates inflammation and vascular leak in a clinically relevant two-hit model of acute lung injury. *Am J Physiol Lung Cell Mol Physiol*. 2015;309(11):L1294-L1304.
41. Dankwa S, Dols MM, Wei L, et al. Exploiting polypharmacology to dissect host kinases and kinase inhibitors that modulate endothelial barrier integrity. *Cell Chem Biol*. 2021;28(12):1679-1692.e4.
42. Darling TK, Mimche PN, Bray C, et al. EphA2 contributes to disruption of the blood-brain barrier in cerebral malaria. *PLoS Pathog*. 2020;16(1):e1008261.
43. Nacer A, Movila A, Baer K, Mikolajczak SA, Kappe SH, Frevert U. Neuroimmunological blood brain barrier opening in experimental cerebral malaria. *PLoS Pathog*. 2012;8(10):e1002982.
44. Lou J, Lucas R, Grau GE. Pathogenesis of cerebral malaria: recent experimental data and possible applications for humans. *Clin Microbiol Rev*. 2001;14(4):810-820.
45. Strangward P, Haley MJ, Shaw TN, et al. A quantitative brain map of experimental cerebral malaria pathology. *PLoS Pathog*. 2017;13(3):e1006267.

46. Carroll RW, Wainwright MS, Kim KY, et al. A rapid murine coma and behavior scale for quantitative assessment of murine cerebral malaria. *PLoS One*. 2010;5(10):e13124.

47. Inoue A, Imamura CK, Shimada H, et al. Pharmacokinetics, efficacy and safety of bosutinib in a pediatric patient with chronic myeloid leukemia. *J Pediatr Pharmacol Ther*. 2020;25(8):742-745.

48. Tanaka C, Yin OQ, Sethuraman V, et al. Clinical pharmacokinetics of the BCR-ABL tyrosine kinase inhibitor nilotinib. *Clin Pharmacol Ther*. 2010;87(2):197-203.

49. Esser S, Lampugnani MG, Corada M, Dejana E, Risau W. Vascular endothelial growth factor induces VE-cadherin tyrosine phosphorylation in endothelial cells. *J Cell Sci*. 1998;111(Pt 13):1853-1865.

50. Klomp JE, Shaaya M, Matsche J, et al. Time-variant SRC kinase activation determines endothelial permeability response. *Cell Chem Biol*. 2019;26(8):1081-1094.e6.

51. Wallez Y, Cand F, Cruzalegui F, et al. Src kinase phosphorylates vascular endothelial-cadherin in response to vascular endothelial growth factor: identification of tyrosine 685 as the unique target site. *Oncogene*. 2007;26(7):1067-1077.

52. Fu P, Epshtein Y, Ramchandran R, et al. Essential role for paxillin tyrosine phosphorylation in LPS-induced mitochondrial fission, ROS generation and lung endothelial barrier loss. *Sci Rep*. 2021;11(1):17546.

53. Lopez-Colome AM, Lee-Rivera I, Benavides-Hidalgo R, Lopez E. Paxillin: a crossroad in pathological cell migration. *J Hematol Oncol*. 2017;10(1):50.

54. Anastassiadis T, Deacon SW, Devarajan K, Ma H, Peterson JR. Comprehensive assay of kinase catalytic activity reveals features of kinase inhibitor selectivity. *Nat Biotechnol*. 2011;29(11):1039-1045.

55. Storm J, Wu Y, Davies J, Moxon CA, Craig AG. Testing the effect of PAR1 inhibitors on Plasmodium falciparum-induced loss of endothelial cell barrier function. *Wellcome Open Res*. 2020;5:34.

56. Zuniga M, Gomes C, Chen Z, et al. Plasmodium falciparum and TNF-alpha differentially regulate inflammatory and barrier integrity pathways in human brain endothelial cells. *mBio*. 2022;13(5):e0174622.

57. Ananthula HK, Parker S, Touchette E, et al. Preclinical pharmacokinetic evaluation to facilitate repurposing of tyrosine kinase inhibitors nilotinib and imatinib as antiviral agents. *BMC Pharmacol Toxicol*. 2018;19(1):80.

58. Marchiafava E, Bignami A. *Two monographs on malaria and the parasites of malaria fevers*150. London: The New Sydenham Society; 1892.

59. Figueiredo RT, Fernandez PL, Mourao-Sa DS, et al. Characterization of heme as activator of Toll-like receptor 4. *J Biol Chem*. 2007;282(28):20221-20229.

60. Pamplona A, Ferreira A, Balla J, et al. Heme oxygenase-1 and carbon monoxide suppress the pathogenesis of experimental cerebral malaria. *Nat Med*. 2007;13(6):703-710.

61. Mita-Mendoza NK, van de Hoef DL, Lopera-Mesa TM, et al. A potential role for plasma uric acid in the endothelial pathology of Plasmodium falciparum malaria. *PLoS One*. 2013;8(1):e54481.

62. Orengo JM, Evans JE, Bettiol E, Leliwa-Sytek A, Day K, Rodriguez A. Plasmodium-induced inflammation by uric acid. *PLoS Pathog*. 2008;4(3):e1000013.

63. Mantel PY, Marti M. The role of extracellular vesicles in Plasmodium and other protozoan parasites. *Cell Microbiol*. 2014;16(3):344-354.

64. Gillrie MR, Krishnegowda G, Lee K, et al. Src-family kinase dependent disruption of endothelial barrier function by Plasmodium falciparum merozoite proteins. *Blood*. 2007;110(9):3426-3435.

65. Craig AG, Grau GE, Janse C, et al. The role of animal models for research on severe malaria. *PLoS Pathog*. 2012;8(2):e1002401.

66. White NJ, Turner GD, Medana IM, Dondorp AM, Day NP. The murine cerebral malaria phenomenon. *Trends Parasitol*. 2010;26(1):11-15.

67. Cabrales P, Zanini GM, Meays D, Frangos JA, Carvalho LJ. Murine cerebral malaria is associated with a vasospasm-like microcirculatory dysfunction, and survival upon rescue treatment is markedly increased by nimodipine. *Am J Pathol*. 2010;176(3):1306-1315.

68. Desruisseaux MS, Machado FS, Weiss LM, Tanowitz HB, Golightly LM. Cerebral malaria: a vasculopathy. *Am J Pathol*. 2010;176(3):1075-1078.

69. Gallego-Delgado J, Basu-Roy U, Ty M, et al. Angiotensin receptors and beta-catenin regulate brain endothelial integrity in malaria. *J Clin Investig*. 2016;126(10):4016-4029.

70. Gordon EB, Hart GT, Tran TM, et al. Targeting glutamine metabolism rescues mice from late-stage cerebral malaria. *Proc Natl Acad Sci U S A*. 2015;112(42):13075-13080.

71. Mota S, Bensalel J, Park DH, Gonzalez S, Rodriguez A, Gallego-Delgado J. Treatment reducing endothelial activation protects against experimental cerebral malaria. *Pathogens*. 2022;11(6):643.

72. Serghides L, McDonald CR, Lu Z, et al. PPARγ agonists improve survival and neurocognitive outcomes in experimental cerebral malaria and induce neuroprotective pathways in human malaria. *PLoS Pathog*. 2014;10(3):e1003980.

73. Eckart F, Tauer JT, Suttorp M, Knofler R. Impact of tyrosine kinase inhibitors applied for first-line chronic myeloid leukemia treatment on platelet function in whole blood of healthy volunteers in vitro. *Hamostaseologie*. 2023;43(3):179-187.

74. Zhang Y, Yang CJ, Melrose AR, et al. Pharmacological effects of small molecule BCR-ABL tyrosine kinase inhibitors on platelet function. *J Pharmacol Exp Ther*. 2025;392(1):100020.

75. Swanson PA 2nd, Hart GT, Russo MV, et al. CD8+ T cells induce fatal Brainstem pathology during cerebral malaria via luminal antigen-specific engagement of brain vasculature. *PLoS Pathog*. 2016;12(12):e1006022.

76. Haque A, Best SE, Unosson K, et al. Granzyme B expression by CD8+ T cells is required for the development of experimental cerebral malaria. *J Immunol*. 2011;186(11):6148-6156.

77. Howland SW, Poh CM, Gun SY, et al. Brain microvessel cross-presentation is a hallmark of experimental cerebral malaria. *EMBO Mol Med*. 2013;5(7):984-999.

78. Nitcheu J, Bonduelle O, Combadiere C, et al. Perforin-dependent brain-infiltrating cytotoxic CD8+ T lymphocytes mediate experimental cerebral malaria pathogenesis. *J Immunol*. 2003;170(4):2221-2228.

79. Qin J, Lovelace MD, Mitchell AJ, de Koning-Ward T, Grau GE, Pai S. Perivascular macrophages create an intravascular niche for $CD8^+$ T cell localisation prior to the onset of fatal experimental cerebral malaria. *Clin Transl Immunology*. 2021;10(4):e1273.

80. Blake SJ, Lyons AB, Hughes TP. Nilotinib inhibits the Src-family kinase LCK and T-cell function in vitro. *J Cell Mol Med*. 2009;13(3):599-601.

81. Chen J, Schmitt A, Chen B, et al. Nilotinib hampers the proliferation and function of CD8+ T lymphocytes through inhibition of T cell receptor signalling. *J Cell Mol Med*. 2008;12(5B):2107-2118.

82. Nampota-Nkomba N, Nyirenda OM, Mallewa J, et al. DON in pediatric cerebral malaria, a phase I/IIA dose-escalation safety study: study protocol for a clinical trial. *Trials*. 2024;25(1):87.

83. Dondorp AM, Nosten F, Yi P, et al. Artemisinin resistance in Plasmodium falciparum malaria. *N Engl J Med*. 2009;361(5):455-467.